El Cezeri
Journal of Science and Engineering
ISSN: 2148-3736

Research Article

3E Analysis of Ejector Compression Absorption Cascade Cycle Working with Environmental Friendly Refrigerants

Billal Mebarki[1a]
[1]Laboratory of Built Environment, Department of Structures and Materials, Faculty of Civil Engineering, University of Science and Technology HouariBoumedien (USTHB), BP 32 Bab Ezzouar 16111, Alger, Algeria Adress: Algiers, Algeria

billal.mebarki@usthb.edu.dz

DOI : 10.31202/ecjse.1696630
Received: 10.05.2025 Accepted: 08.12.2025
How to cite this article:
Billal Mebarki, "3E Analysis of Ejector Compression Absorption Cascade Cycle Working with Environmental Friendly Refrigerants ", El-Cezeri Journal of Science and Engineering, Vol: 13, Iss: 1, (2026), pp.(112-124).
ORCID: [a]0000-0002-0364-6101.

Abstract The absorption–compression cascade cycle requires minimal electricity and effectively utilizes low-grade thermal energy, making it a promising option for efficient refrigeration. In this study, the performance of an ejector-assisted compression–absorption cascade cycle was evaluated using eleven eco-friendly refrigerants that are ozone-friendly and have low global warming potential in the vapor-compression stage. The results indicated that carbon dioxide exhibited the highest performance and the greatest energy efficiency among the investigated refrigerants. Additionally, the influence of generator temperature on system performance was analyzed, and the main sources of exergy destruction were identified. Annual costs were calculated by combining investment, operational, and environmental expenses. The findings revealed that system performance reached its optimum at a specific generator temperature and declined as the temperature increased further, whereas annual costs followed the opposite trend. The absorber, generator, two heat exchangers, and condenser accounted for the majority of the exergy losses, while the compressor and ejector contributed less. Overall, the results demonstrate the system's strong potential for improving both energy efficiency and cost-effectiveness in environmentally sustainable refrigeration applications

Keywords: Absorption, Cascade, Cop, Ejector, Exergy, Vapor compression.

1. INTRODUCTION

The refrigeration cycle is one of the major consumers of electrical energy and contributes significantly to environmental pollution due to the use of refrigerants with high Global Warming Potential (GWP), a measure of how much heat a greenhouse gas traps in the atmosphere during heat transfer in refrigeration systems. The absorption–compression cascade cycle, which combines absorption and compression refrigeration processes in sequence, has emerged as a promising solution to reduce electrical consumption and mitigate the environmental impact of refrigeration systems[1]

Numerous researchers have conducted in-depth evaluations of absorption–compression cascade cycles to explore their energy efficiency, exergy performance, and potential for effective recovery and utilization of low-grade thermal energy. Khelifa et al. [1] simulated a compression–absorption cascaded cycle using various refrigerants R1234yf, R1234ze(E), and R1233zd(E)for the compression section, and Lithium Chloride LiCl–H_2O and Lithium Bromide LiBr–H_2O working pairs for the absorption section. The generator heat was supplied from geothermal sources in Algeria. Their results showed that this configuration reduced electrical energy consumption by 51.34–54.16 % compared with the conventional vapor-compression cycle under similar conditions. Du et al. [2]studied a similar system with sixteen refrigerants in the compression stage and LiBr–H_2O in the absorption stage, concluding that refrigerant RE170 achieved the highest exergy efficiency and coefficient of performance (COP).

Recent investigations have focused on enhancing system performance through the integration of ejectors and the implementation of multi-stage configurations. Khan et al. [3]demonstrated that introducing an ejector in the compression stage tripled the COP compared with a conventional compression–absorption cascade cycle using R134a. Zhang et al. [4]proposed a two-stage compression–absorption configuration with a flash tank, achieving 31.6 % and 41.7 % improvements in COP and exergy efficiency, respectively.

Environmental regulations have accelerated the transition toward low-GWP refrigerants. Since 2022, the European Commission has limited refrigerants with GWP values above 150 in most systems, except for primary fluids in cascade configurations where values up to 1500 are allowed [5]. The U.S. Environmental Protection Agency designated 2016 as the final production year for systems utilizing R410A[6], whereas California regulations will progressively reduce GWP thresholds to 2200 by 2025, 1500 by 2030, and 750 by 2033 [7]. Widely used refrigerants, including R410A and R134a, not

only exhibit high GWP values but also present multiple challenges, such as flammability, toxicity, thermal instability, corrosiveness, and elevated costs [8]. Conversely, carbon dioxide (CO_2) is non-toxic, non-flammable, non-corrosive, abundant, and inexpensive, with an Ozone Depletion Potential (ODP) of zero and a GWP of one [9]. In this study, eleven low-GWP refrigerants are compared to identify the most suitable candidate for the Ejector Compression Absorption Cascade Cycle (ECACC).

Among absorption working pairs, ammonia–water (NH_3–H_2O) and lithium bromide–water (LiBr–H_2O) are the most extensively employed due to their proven thermodynamic stability and favorable performance characteristics. Cimsit and Ozturk [10] reported that a LiBr–H_2O-based cascade system achieved a COP approximately 33 % higher than that of NH_3–H_2O for the same cooling capacity. Seyfouri and Ameri [11] observed that NH_3–H_2O systems require higher generator pressure, leading to greater pump power consumption. Consequently, the LiBr–H_2O pair is selected for the absorption section in this study.

Recent research trends in absorption–compression cascade refrigeration have focused on thermodynamic optimization, exergy-based diagnostics, and hybrid cycle configurations. Bahrami and Fazli [12] compared several cascade architectures and found that incorporating an ejector reduced compressor work by 18% and improved the coefficient of performance (COP) by up to 15%, while simultaneously lowering the total exergy destruction by 11%. Dixit [13]reported that employing LiBr–H_2O as the working pair in the absorption stage minimized total exergy destruction and achieved a 6 % higher exergy efficiency than NH_3–H_2O under the same operating conditions. Özen and Yağcıoğlu [14]achieved an exergy efficiency of 40.5 % and a COP of 0.82 for LiBr–H_2O single-effect systems operating at generator temperatures of 90–95 °C, while noting that performance decreased sharply beyond 100 °C due to crystallization effects. Liu et al. [15] applied advanced exergy analysis to identify the generator and absorber as the dominant sources of avoidable exergy destruction, accounting for nearly 60% of total losses, and suggested that optimizing heat exchanger effectiveness could improve overall exergy efficiency by up to 10%. Kumar and Modi [16]developed an ejector-assisted compression–absorption–resorption cycle that increased exergy efficiency by 12 % and COP by 9.5 %, primarily by recovering expansion losses through the ejector and resorption stages. Yuksel [17] investigates a geothermal-based multi-generation plant that integrates an absorption refrigeration cycle to provide simultaneous cooling, heating, and power. The study demonstrates that absorption cycles effectively utilize low-grade geothermal heat, enhancing both energy and exergy efficiency. Overall, the system reduces primary energy consumption and environmental impact compared to conventional separate-generation setups. Okwose et al. [18]examined solar-powered, compressor-assisted combined absorption refrigeration and power systems, evaluating single-, double-, and triple-effect configurations. Their results show that the triple-effect cycle significantly improves both the Coefficient of Performance and exergy efficiency, allowing more efficient use of low-grade thermal energy sources. Faruque et al. [19]concluded that the R41/LiBr–H_2O combination offers the best trade-off between thermodynamic performance, system cost, and environmental impact, achieving a COP of 18.49 % and exergy efficiency of 46.8 %. Furthermore, Mukhtar and Ghani [20]emphasized the potential of artificial neural networks (ANNs) for predicting and optimizing hybrid ejector–absorption systems, achieving prediction accuracies above 98 % and demonstrating that ANN-guided optimization can improve system COP by up to 8 % compared to classical thermodynamic models.

In this work, the Ejector Compression Absorption Cascade Cycle (ECACC) is modeled using the first and second laws of thermodynamics to establish mass, energy, and exergy balances for each component. The proposed configuration integrates an ejector to decrease the refrigerant mass flow entering the compressor, thereby reducing compressor work, and includes a liquid–vapor heat exchanger to enhance internal heat recovery. An economic assessment of annual cost and environmental impact is also performed. This study systematically evaluates the effect of generator temperature, analyzes the distribution of exergy destruction, and assesses component investment costs to identify the principal factors influencing system optimization and guiding future development.

2. CYCLE DESCRIPTION

Figure 1 illustrates the Ejector–Compression Absorption Cascaded Cycle (ECACC), which consists of the following components: a generator, absorber, condenser, solution pump, solution heat exchanger, cascade heat exchanger, liquid–vapor heat exchanger, evaporator, ejector, separator tank, compressor, two expansion valves, and a pressure-reduction valve.

In the absorption cycle, the saturated refrigerant vapor leaves the generator at point (16) and condenses in the condenser, which is cooled by circulating water. At the condenser outlet at point (5), the refrigerant is in a saturated liquid state and is subcooled in the liquid–vapor heat exchanger to point (6). It is then expanded through Expansion Valve 1, reducing the pressure from the condensation level to the evaporation pressure of the absorption cycle at point (7). The resulting two-phase mixture enters the cascade heat exchanger, where it absorbs thermal energy from the refrigerant of the ejector–compression cycle. Consequently, the absorption-cycle refrigerant undergoes vaporization and exits the exchanger as saturated vapor at point (8).

The saturated vapor leaving the cascade heat exchanger is further heated in the liquid–vapor heat exchanger to point (9) before entering the absorber, where it is absorbed by the weak solution arriving through the pressure-reduction valve at point (15). This process generates a strong solution that exits the absorber at point (10) and is subsequently pressurized to the generator level by the solution pump at point (11). The strong solution is preheated in the solution heat exchanger by the hot

weak solution returning from the generator. After releasing heat, the weak solution at point (14) is expanded through the reduction valve to the evaporation pressure at point (15) and re-enters the absorber, thereby completing the absorption-cycle loop.

In the ejector-compression cycle, part of the refrigerant vapor leaving the separator tank at point (1) is compressed from the intermediate to the high pressure by the compressor at point (2). The high-pressure vapor is then cooled in the cascade heat exchanger, where it transfers heat to the absorption-cycle refrigerant and exits at point (3). This cooled vapor is mixed with another vapor stream that originates from the evaporator formed when the liquid refrigerant from the separator tank is expanded through Expansion Valve 2 and evaporates at low pressure. The two streams mix in the ejector, where the high-velocity primary flow entrains the secondary vapor flow. The mixed refrigerant leaves the diffuser section of the ejector at point (25) and enters the separator tank, where vapor–liquid separation occurs, completing the ejector-compression cycle.

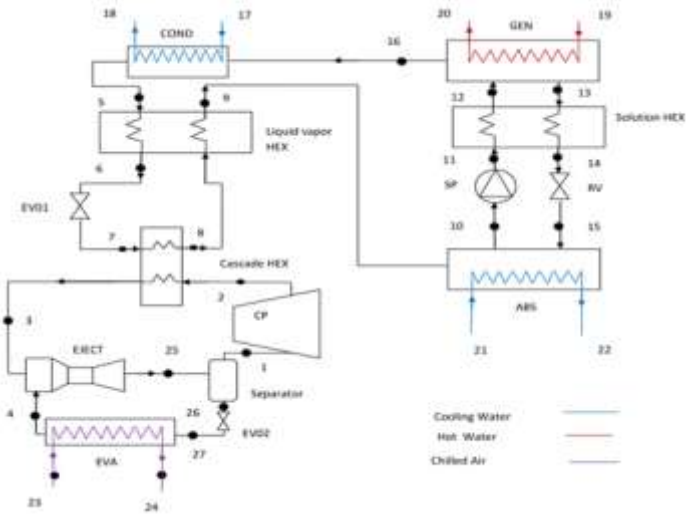

Figure1. Schematic of Ejector Compression Absorption Cascade Cycle (ECACC).

3. THERMODYNAMIC CYCLE MODELING

3.1. Ejector Model

The one-dimensional model with constant pressure in the mixing section is used in this study. The simplicity assumptions are the following [21]

- There is no exchange of heat between the ejector and exterior.
- The velocities, primary and secondary fluid velocities in the inlet of the ejector, are neglected.
- The velocity of the fluid at the outlet of the ejector is neglected.
- The efficiency of different sections of the ejector, like the nozzle, mixing, and diffuser sections, is considered constant.
- The refrigerant flow losses in the ejector are taken into account by using different ejector section efficiencies.

Table 1. The thermo physical propriety calculated model of ejector used.

Thermo physical propriety	Model used	Reference
The primary fluid velocity at the nozzle chamber outlet	$U_{n,out}=\sqrt{\eta_n.(h_{p,in}-h_{n,out,is}).1000}$	[21]
The fluid velocity at the outlet of the mixing chamber	$U_{m,out}=\frac{U_{n,out}}{1+\mu}\sqrt{\eta_m}$	[21]
The fluid enthalpy at the outlet of the mixing chamber	$h_{m,out}=\frac{h_{n,in}+\mu.h_{s,in}}{1+\mu}-(\frac{U_{n,out}^2}{2})/1000$	[21]
The ejector entrainment ratio	$\mu=\frac{\dot{m}_p}{\dot{m}_s}$	[21]
The outlet diffuser chamber enthalpy	$h_{d,out}=h_{m,out}+\frac{h_{d,out,is}-h_{m,out}}{\eta_d}$	[21]
The evaluation of the ejector entrainment ratio	$\mu=\sqrt{\eta_n.\eta_m.\eta_d\frac{h_{p,in}-h_{m,out,is}}{h_{d,out,is}-h_{m,out}}}-1$	[21]

The conservation laws of energy, mass, and momentum were applied to the various sections of the ejector—specifically, the nozzle, mixing chamber, and diffuser—based on the aforementioned assumptions. The thermo physical parameters of the ejector are summarized in Table 1.

Where U is the primary fluid velocity, $h_{p,in}$ is the primary fluid enthalpy at the inlet of the nozzle chamber, η_n is the isentropic efficiency of the nozzle chamber, in is the inlet, out is the outlet and the is the isentropic expansion, $h_{s,in}$ is the secondly fluid enthalpy at the nozzle chamber inlet and η_d is the efficiency of the diffuse chamber.

3.2. Thermodynamic Model

In this study, each component of the ejector-assisted compression–absorption cascade cycle is modeled using its inlet and outlet state points. The energy and exergy balances are defined based on the first and second laws of thermodynamics, as well as the mass conservation law, to analyze the system's thermodynamic performance. The following simplified assumptions are made:

- The proposed cycle operates under steady-state conditions [22], [23]
- Except for the ejector, pressure losses in all cycle components are considered negligible [22]
- No heat exchange occurs between the cycle and the environment, except for that explicitly accounted for in the study [22]
- The outlet state of the refrigerant from the condenser, evaporator, and cascade heat exchanger is saturated liquid, vapor, and saturated vapor, respectively [22]
  The work of the solution pump is neglected in the calculation of the performance coefficient and exergy efficiency due to its very low value [14, 17, 18]

3.2.1. Mass Conservation

The mass conservation of the refrigerant and solution in each component of the ejector-assisted compression–absorption cascade cycle (ECACC) is expressed by the following equations [24]

$$\sum \dot{m}_i - \sum \dot{m}_0 = 0 \tag{1}$$

$$\sum \dot{m}_i . x_i - \sum \dot{m}_0 . x_0 = 0 \tag{2}$$

Where $\dot{m}$ is the mass flow rate and x is is the lithium bromide mass fraction in the solution.

3.2.2. The First Law of Thermodynamics

The first law of thermodynamics is systematically applied to each component of the proposed ECACC to evaluate its energy balance, as outlined in [24]

$$\left(\sum \dot{m}_i . h_i - \sum \dot{m}_0 . h_0\right) + \left(\sum \dot{Q}_i - \sum \dot{Q}_0\right) - \dot{W} = 0 \tag{3}$$

Where h is the specific enthalpy, $\dot{Q}$ is heat exchanged, and $\dot{W}$ is the mechanical work to or from to component.

The energy balance equations of components of ECACC are presented in Table 2.

3.2.3. The Second Law of Thermodynamics

The aim of the exergy study is to analyze the irreversibility's of the entire cycle and its individual components using the second law of thermodynamics to optimize performance. In this study, chemical, kinetic, and potential exergy are neglected, and only physical exergy is considered [2]. The exergy destruction of each component of the ECACC can be defined as follows [24]

$$\dot{Ex}_d = \sum_j \dot{Q}_j . \left(1 - \frac{T_0}{T_i}\right) + \left(\sum_i \dot{m}_i . ex_i\right)_{in} - \left(\sum_i \dot{m}_i . ex_i\right)_{out} - \dot{W} \tag{4}$$

Where, ex_i is the specific exergy at each point of ECACC, which is calculated by the following equation [24]

$$ex_i = (h_i - h_0) - T_0 . (s_i - s_0) \tag{5}$$

Where h_0, T_0 and s_0 are representing the specific enthalpy, temperature, and specific entropy of reference environmental state which are T_0=25 °C and P_0= 101kPa.

The different component of ECACC exergy destruction is presented in Table 3.

The destruction exergy of the ECACC cycle $\dot{Ex}_{dt}$ is the sum of the exergy destruction of its different components. It can be calculated by following the equation [24]

Table2. The energy balance of different components of ECACC.

Cycle component	The energy balance
Generator	$\dot{Q}_g=\dot{m}_{13}.h_{13}+\dot{m}_{16}.h_{16}-\dot{m}_{12}.h_{12}$
Absorber	$\dot{Q}_a=\dot{m}_9.h_9+\dot{m}_{15}.h_{15}-\dot{m}_{10}.h_{10}$
Condenser	$\dot{Q}_c=\dot{m}_{16}.h_{16}-\dot{m}_5.h_5$
Cascade heat exchanger	$\dot{Q}_{chx}=\dot{m}_8.h_8-\dot{m}_7.h_7$
Evaporator	$\dot{Q}_e=\dot{m}_4.h_4-\dot{m}_{27}.h_{27}$
Expansion valve 01	$h_6=h_7$
Expansion valve 02	$h_{26}=h_{27}$
Reducing valve	$h_{14}=h_{15}$
Solution Heat exchanger	$h_{14}=h_{13}-\varepsilon_{she}.(h_{13}-h_{11})$
	$h_{12}=\frac{\dot{m}_{13}}{\dot{m}_{11}}.(h_{13}-h_{14})+h_{11}$
Liquid vapor heat exchanger	$h_6=h_5-\varepsilon_{che}.(h_5-h_8)$
	$h_8=\frac{\dot{m}_5}{\dot{m}_7}.(h_5-h_6)+h_7$
Compressor	$\dot{W}_{com}=\dot{m}_1.\frac{h_{2,is}-h_1}{\eta_{is,\,com}.\eta_{el}}$

$$\dot{Ex}_{dt}=\sum \dot{Ex}_i \tag{6}$$

The exergy efficiency of the presented cycle is calculated by following equation [24]

$$\eta_{ex}=\frac{\dot{Q}_{ev}.\left(1-\frac{T_0}{T_{ev}}\right)}{\dot{Q}_g.\left(1-\frac{T_0}{T_g}\right)+\dot{W}_{com}} \tag{7}$$

The coefficient performance of the ECACC cycle can be found using the following equation:

$$COP=\frac{\dot{Q}_{ev}}{\dot{Q}_g.+\dot{W}_{com}} \tag{8}$$

Table 3. The exergy destruction of different components of ECACC.

Cycle component	The destruction exergy
Generator	$\dot{Ex}_g=\dot{m}_{12}.ex_{12}+\dot{m}_{19}.ex_{19}-\dot{m}_{13}.ex_{13}-\dot{m}_{16}.ex_{16}-\dot{m}_{20}.ex_{20}$
Absorber	$\dot{Ex}_a=\dot{m}_9.ex_9+\dot{m}_{15}.ex_{15}+\dot{m}_{21}.ex_{21}-\dot{m}_{10}.ex_{10}-\dot{m}_{22}.ex_{22}$
Condenser	$\dot{Ex}_c=\dot{m}_{16}.ex_{16}+\dot{m}_{17}.ex_{17}-\dot{m}_5.ex_5-\dot{m}_{18}.ex_{18}$
Cascade heat exchanger	$\dot{Ex}_{chex}=\dot{m}_2.ex_2+\dot{m}_7.ex_7-\dot{m}_3.ex_3-\dot{m}_8.ex_8$
Evaporator	$\dot{Ex}_e=\dot{m}_{23}.ex_{23}+\dot{m}_{26}.ex_{26}-\dot{m}_4.ex_4-\dot{m}_{24}.ex_{24}$
Expansion valve 01	$\dot{Ex}_{ev1}=\dot{m}_6.T_0.(S_6-S_7)$
Expansion valve 02	$\dot{Ex}_{ev2}=\dot{m}_{26}.T_0.(S_{26}-S_{27})$
Heat exchanger	$\dot{Ex}_{hx}=\dot{m}_{11}.ex_{11}+\dot{m}_{13}.ex_{13}-\dot{m}_{12}.ex_{12}-\dot{m}_{14}.ex_{14}$
Liquid vapor heat exchanger	$\dot{Ex}_{lvhex}=\dot{m}_5.ex_5+\dot{m}_8.ex_8-\dot{m}_6.ex_6-\dot{m}_9.ex_9$
Compressor	$\dot{Ex}_{com}=\dot{m}_1.ex_1-\dot{m}_2.ex_2+\dot{W}_{com}$
Ejector	$\dot{Ex}_{ej}=\dot{m}_3.ex_3+\dot{m}_4.ex_4-\dot{m}_{25}.ex_{25}$

In Table 4, the design input used in the simulations of ECACC performance

3.3. The Economic Study

The economic study includes the analysis of investment, operating, and maintenance costs of ECACC and studies the effect of some operating parameters on the ECACC cost, which is defined by [25]

$$C_T=t_{op}.\left(C_f\dot{Q}_g+C_{ele}.\dot{W}_{comp}\right)+C_r.M.\sum Z_i+C_{env} \tag{9}$$

Where, C_T is the cost total of ECACC, t_{op} is the annual operation time, C_f is the cost of fuel of generation heat, C_{ele} is the cost of electrical energy, M is the factor of maintenance, Z_i in the investment cost of each component of ECACC, C_{env} is the social cost of CO_2 emission of ECACC, and C_r is the factor of capital recovery which is calculated by the following equation [4]

Table 4. Design input table.

Parameter	Value	Parameter	Value
Colling power $\dot{Q}_{ev}$	250 kW	Chiled air temperature outlet T_{24}	266.15 K
Temperature of generatorT_g	360.15 K	Pinch of evaporator ΔT_{eva}	8 K
Temperature inlet of water to CHE T_7	283.15 K	Pinch of condenserΔT_{con}	8 K
Condenser cooling water inlet T_{17}	300.15 K	Pinch of generatorΔT_{gen}	8 K
Condenser cooling water outlet T_{18}	305.15 K	Pinch of absorber ΔT_{abs}	8 K
Hot water generator inlet T_{19}	378.15 K	Pinch of cascade heat exchanger ΔT_{che}	8 K
Hot water generator outlet T_{20}	368.15 K	Solution heat exchanger efficiency ε_{she}	0.7
Absorber cooling water inlet T_{21}	300.15 K	Liquid vapor heat exchanger efficiency ε_{Lvhe}	0.7
Absorber cooling water outletlet T_{22}	305.15 K	Isontropic compressor efficiency $\eta_{is.com}$	0.8
Chiled air temperature inlet T_{23}	271.15 K	Electrical compressor efficiency $\eta_{el.com}$	0.9

$$C_r = \frac{i.(i+1)^L}{(i+1)^L - 1} \tag{10}$$

Where, i is the rate of interest annual and L is the life time of ECACC

The main component type of ECACC is heat exchangers, where its investment cost is very dependent on its area, which can be concluded using the following equation:

$$Q_i = U_i.\, A_i.LMTD_i \tag{11}$$

Where LMTD is the logarithmic mean temperature difference, and it can be calculated with the following equation:

$$LMTD_i = \frac{\Delta T_i^H - \Delta T_i^c}{\ln\left(\frac{\Delta T_i^H}{\Delta T_i^c}\right)} \tag{12}$$

The various heat transfer coefficients and the logarithmic mean temperature difference (LMTD) of the ECACC heat exchangers are presented in Table 5.

The investment cost of the heat exchangers can be calculated using the following equation [26]:

$$Z_{invi} = 516{,}62.\, A_i. + 268{,}45 \tag{13}$$

The investment cost of the compressor can be defined as [2]

$$Z_{inv\text{-}comp} = \left(\frac{573.m_1}{0{,}8996 - \eta_{is,com}}\right).\left(\frac{P_1}{P_2}\right).ln\left(\frac{P_1}{P_2}\right) \tag{14}$$

The investment cost of the ejector can be calculated as [29]

$$Z_{inv\text{-}eje} = 750.\dot{m}_3.\left(\frac{T_3}{P_3}\right)^{0{,}05}.\left(\frac{P_{25}}{1000}\right)^{-0.75} \tag{15}$$

3.4. The Environmental Study

With increasingly strict environmental regulations, the study of CO_2 emissions has become a crucial factor in selecting refrigerants. The annual CO_2 emissions can be determined using the following equation[30],[31]

$$m_{co2} = ECF.\, t_{op}.\dot{W}_{com} \tag{16}$$

Where, ECF is the emission conversion factor of electricity.

The environmental cost can be calculated by following equation [30], [31]

$$C_{env} = \mu_{co2}.\frac{m_{co2}}{1000} \tag{17}$$

Where, μ_{co2} is the CO2 emission unit damage cost.

The main parameters used in the economy and environmental studies are presented in Table 6

Table 5. The heat exchanger coefficient and LMTD of different ECACC heat exchangers [27], [28]

Component	U(kW·(m^2·K)$^{-1}$)	*LMTD*
Generator	1,5	$LMTD_{gen}=\frac{(T_{19}-T_{12})-(T_{20}-T_{13})}{\ln(\frac{T_{19}-T_{12}}{T_{20}-T_{13}})}$
Absorber	0,7	$LMTD_{abs}=\frac{(T_{15}-T_{22})-(T_{10}-T_{21})}{\ln(\frac{T_{15}-T_{22}}{T_{10}-T_{21}})}$
Condenser	2,5	$LMTD_{cond}=\frac{(T_{5}-T_{17})-(T_{5}-T_{18})}{\ln(\frac{T_{5}-T_{17}}{T_{5}-T_{18}})}$
Solution heat exchanger	1	$LMTD_{SHE}=\frac{(T_{12}-T_{13})-(T_{11}-T_{14})}{\ln(\frac{T_{12}-T_{13}}{T_{11}-T_{14}})}$
Liquid vapor heat exchanger	1	$LMTD_{LVE}=\frac{(T_{5}-T_{9})-(T_{6}-T_{8})}{\ln(\frac{T_{5}-T_{9}}{T_{6}-T_{8}})}$
Cascade heat exchanger	0,55	$LMTD_{CHE}=T_3-T_8$
Evaporator	1,5	$LMTD_{EVA}=\frac{(T_{23}-T_{4})-(T_{24}-T_{4})}{\ln(\frac{T_{23}-T_{4}}{T_{24}-T_{4}})}$

Table 6. The economic and environmental parameters used in this work.

Parameter	*Value*	*ref*
rate of interest annual i	10%	[32]
Life time L	15 years	[32]
Factor of maintenance M	1.06	[26]
annual operation time t_{op}	6000 h	[30]
emission conversion factor of electricity ECF	0,968 kg. (kWh)$^{-1}$	[33]
cost of fuel of generation heat C_f	0 03785 \$. (kWh)$^{-1}$	[2]
cost of electrical energy C_e	0 0375 \$. (kWh)$^{-1}$	[2]
CO2 emission unit damage cost μ_{co2}	90 \$.(ton)$^{-1}$	[31]

4. RESULT AND DISCUSSION

The performance of the ECACC was simulated using a program developed in the Engineering Equation Solver (EES). Based on the thermodynamic, economic, and environmental models described above, the simulation workflow is shown in Figure 2.

The ejector entrainment ratio was determined iteratively, starting with an arbitrary initial value. The fluid states at the outlets of the ejector's nozzle, mixing chamber, and diffuser were calculated using the equations in Table 1. A new entrainment ratio was then computed using the last equation in Table 1, and the iteration continued until the difference between successive values was less than 10^{-4}, at which point the final value was taken as the actual entrainment ratio.

After defining the entrainment ratio, the mass flow through the ECACC components is determined using the entrainment ratio and the ejector's secondary fluid flow, corresponding to the evaporator mass flow. Equations from Tables 2 and 3 are then applied to calculate the energy and exergy destruction of all ECACC components, respectively.

4.1. Model Validation

Validation of the ECACC is not yet possible due to the absence of literature on this new configuration. In this study, validation is performed using two approaches: first, by comparing the conventional compression–absorption cascade cycle without the ejector and liquid–vapor heat exchanger with the results reported by [2]and presented in Figure 3; and second, by validating the ejector model independently. The results of the conventional compression–absorption cascade cycle obtained in this study are compared with those reported by [2], using R134a and R744 as refrigerants in the vapor-compression section. The comparison under identical operating conditions is summarized in Table 8, with the input design parameters listed in Table 7.

Table 8 provides a direct comparison between the results obtained in this work and those reported in [2].

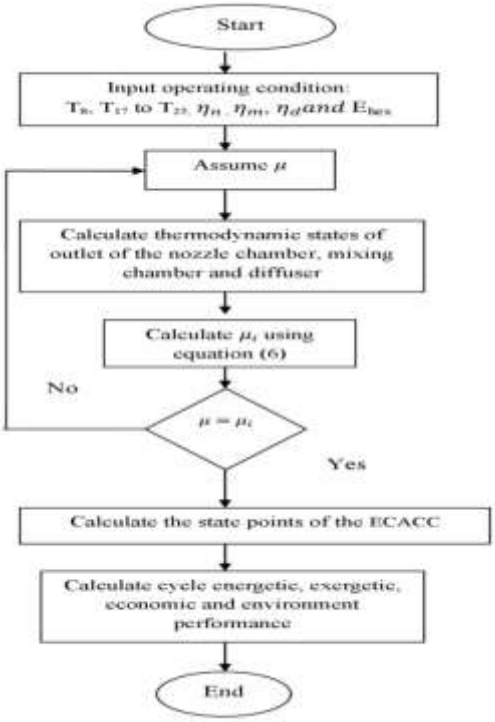

Figure 2. The simulation calculation flowchart.

Table 7. Design input parameter used in comparison with [2]

Parameter	Value	Parameter	Value
Colling power $\dot{Q}_{ev}$	250 kW	Chiled air temperature outlet T_{24}	266.15 K
Temperature of generator T_g	360.15 K	Pinch of evaporator ΔT_{eva}	8 K
Temperature inlet of water to CHE T_7	283.15 K	Pinch of condenser ΔT_{con}	8 K
Condenser cooling water inlet T_{17}	300.15 K	Pinch of generator ΔT_{gen}	8 K
Condenser cooling water outlet T_{18}	305.15 K	Pinch of absorber ΔT_{abs}	8 K
Hot water generator inlet T_{19}	378.15 K	Pinch of cascade heat exchanger ΔT_{che}	8 K
Hot water generator outlet T_{20}	368.15 K	Solution heat exchanger efficiency ε_{she}	0.7
Absorber cooling water inlet T_{21}	300.15 K	Liquid vapor heat exchanger efficiency ε_{Lvhe}	0.7
Absorber cooling water outletlet T_{22}	305.15 K	Isontropic compressor efficiency $\eta_{is.com}$	0.8
Chiled air temperature inlet T_{23}	271.15 K	Electrical compressor efficiency $\eta_{el.com}$	0.9

Table 8. Comparison of results obtained from this work and from [2](COP_{ABS} : COP of absorption cycle, COP_{COM} , COP of vapor compression section, COP_{CCACC} ,COP of CCACC).

Parameters	R134a/H_2O-LiBr			R744/H_2O-LiBr		
	Reference [2]	This work	deviation (%)	Reference [2]	This work	deviation (%)
Heat of generator $\dot{Q}_{GEN\ (kW)}$	362.65	361.3	0.37	376.77	375.4	0.36
Cascade heat exchanger $\dot{Q}_{CHE\ (kW)}$	287.74	287.7	0.01	298.95	299	-0.02
Heat of absorber $\dot{Q}_{ABS\ (kW)}$	344.48	343.1	0.40	357.89	356.5	0.39
Heat of Condenser $\dot{Q}_{CON\ (kW)}$	305.91	305.9	0.00	317.83	317.8	0.01
Work of compressor $\dot{W}_{COM\ (kW)}$	41.91	41.93	-0.05	54.39	54.39	0.00
Absorption cycle :COP_{ABS}	0.794	0.7964	-0.30	0.794	0.7964	-0.30
Compressor vapor cycle :COP_{COM}	5.961	5.962	-0.02	4.597	4.596	0.02
Cascade cycle COP_{CCACC}	0.618	0.62	-0.32	0.58	0.5817	-0.29
Exergy efficiency η_{ex}	0.234	0.2473	-5.68	0.207	0.2174	-5.02

The slight differences between the results of the present study and the numerical results reported in [2]for exergy efficiency are attributed to the methodology used in [2], which considered the average temperature between the inlet and outlet of the evaporator and generator heat exchangers. In contrast, this study calculates exergy efficiency using the commonly adopted formulation based on the actual generator temperature and evaporator temperature. Other parameters show good agreement, with deviations not exceeding 0.3%, indicating that the developed model accurately predicts ECACC system performance.

The ejector model was validated by comparing its results with results obtained from the experimental study [21]and numerical study [34]under identical operating conditions. Table 9 provides a detailed comparison of the experimental results from [21], the numerical results from [34] ,and the results obtained in this study.

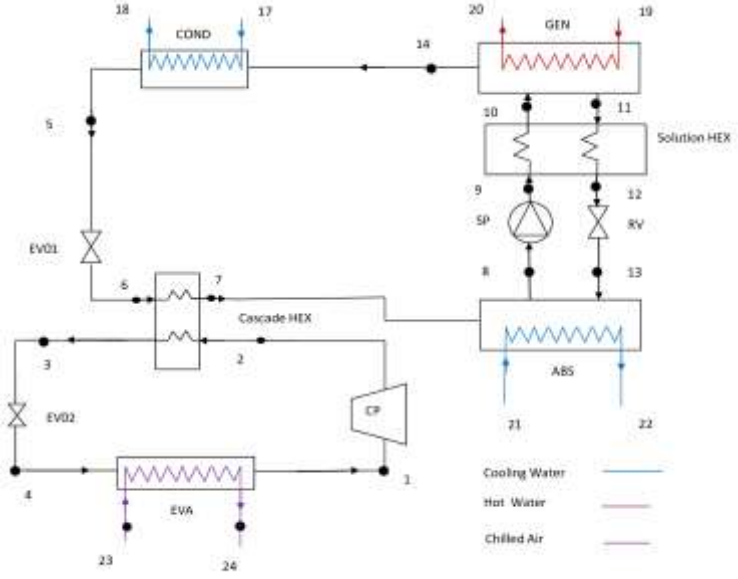

Figure 3. the schematic of the compression absorbed cascade cycle presented by [2].

Table 9. Comparisons of entrainment ratio of the ejector model used in present study with experimental results of [21]and numerical results of [34]

Generator Temperature T_g (°C)	Condenser Temperature T_c (°C)	Entrainment Ratio Experimental [21]	Entrainment Ratio Numerical [34]	Entrainment Ratio This work	Error Experimental (%) [21]	Error Numerical (%) [34]
95	31.3	0.4377	0.4584	0.4473	-2.15	2.48
90	33.8	0.3488	0.3614	0.3507	-0.54	3.05
84	33.6	0.3117	0.3286	0.3182	-2.04	3.27

The entrainment ratio in this study was calculated using a program based on the flow chart shown in Figure 2. Minor differences between these results and those reported in [34]are attributed to variations in calculation methods. However, the results obtained here closely match the experimental data reported in [21], indicating that the developed ejector model accurately represents ejector performance.

4.2. Comparisons of Performance of ECACC

In this section, the studied refrigerants are classified into three groups based on the slope of their cycle on the T–S diagram. The first group includes dry fluids (R600, R600a), the second group comprises isentropic fluids (R1234yf, R1234ze (e), R1243zf), and the third group consists of wet fluids R744, R290, R152A, RE170, R717, R170, and R1270. Table 10 summarizes the global warming potential (GWP) and ozone depletion potential (ODP) of these refrigerants [33], [35], [36], [37].

Figure 4(a) shows the coefficient of performance (COP) and exergy efficiency of the ECACC using dry fluids, with R600a outperforming R600. Figure 4(b) compares ECACC performance with isentropic fluids, revealing slight differences among the refrigerants, with R1234yf achieving the highest performance. The ECACC performance with wet fluids is shown in Figure 4(c), where carbon dioxide (R744) exhibits the highest COP and exergy efficiency across the group and among all studied refrigerants. This behavior is attributed to the dependence of the ejector's entrainment ratio on the pressure difference between the evaporator and compressor outlet pressures, as well as the medium pressure at the ejector outlet, which in turn depends on the refrigerant properties and its saturation pressure.

In the next section, R744 is selected for the compression cycle of the ECACC. Table 11 presents the state-point results under the operating conditions listed in Table 4.

4.3. Effect of Generator Temperature on the Performance of ECACC:

Figure 5 illustrates the effect of generator temperature (T_g) on the total annual cost, coefficient of performance and exergy efficiency of the ECACC. The total cost decreases rapidly with increasing (T_g) up to a certain point and then declines

slightly, while exergy efficiency rises to a maximum before gradually decreasing. The COP increases sharply with (T_g) and stabilizes around 0.82.

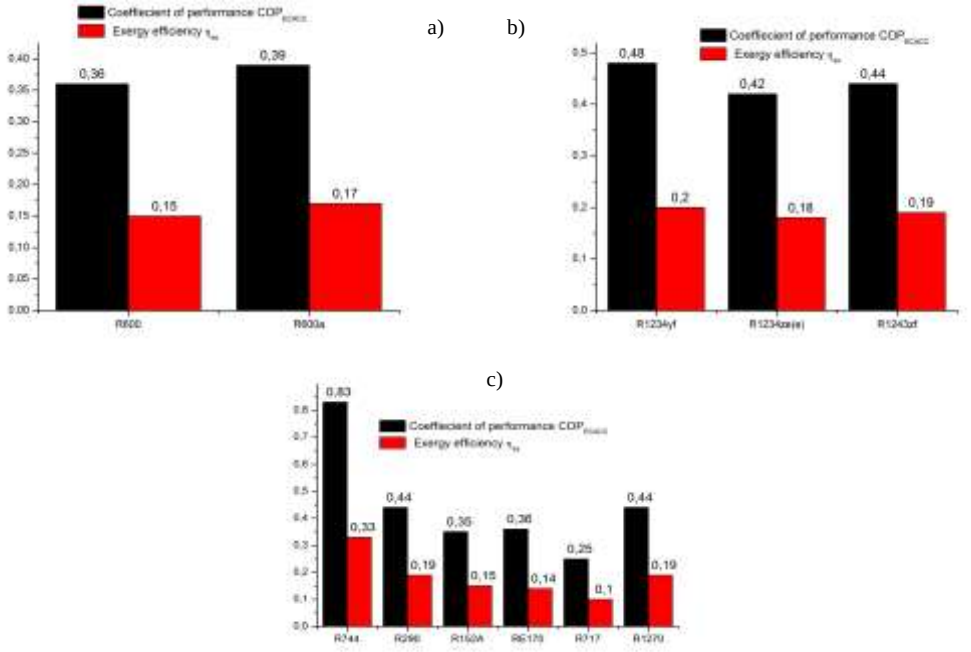

Figure4. The Coefficient of performance and the exergy efficiency of ECACC using: 4-a dry fluids, 4-b isotropic fluids, 4-c wet fluids

Table 10. Global warming potential GWP and Ozone depletion potential ODP of 11 refrigerants used in this work

Refrigerant	Global warming potential GWP	Ozone depletion Potential ODP	Refrigerant	Global warming potential GWP	Ozone depletion Potential ODP
R744	1	0	RE170	0.1	0
R290	20	0	R717	<1	0
R1234yf	4	0	R600	20	0
R1234ze(e)	6	0	R600a	20	0
R1243zf	<150	0	R1270	20	0
R152a	124	0			

Table11. The different properties of proposed cycle state point at optimum operating condition.

Number of state point	Temperature T (K)	Pressure P (kPa)	Enthalpy H (kJ/kg)	Entropy s (kJ/kg.K)	LiBr concentration X (g/kg)	Mass Flow $\dot{m}$ (kg/sec)
1	265	2791	-72.21	-0.85		1.013
2	318	5465	-38.84	-0.8285		1.013
3	291.2	5465	-257.5	-1.573		1.013
4	263.2	2649	-71.64	-0.8405		0.9828
5	308.2	5.629	146.6	0.5051		0.09058
6	290.7	5.629	73.45	0.2606		0.09058
7	283.2	1.228	73.45	0.2621		0.09058
8	283.2	1.228	2519	8.9		0.09058
9	323.8	1.228	2592	9.152		0.09058
10	308.2	1.228	76.13	0.2415	0.5219	0.5111
11	308.2	5.629	76.13	0.2415	0.5219	0.5111
12	338.1	5.629	131.9	0.4392	0.5219	0.5111
13	360.2	5.629	226.1	0.4758	0.6344	0.4205
14	323.8	5.629	158.3	0.22787	0.6344	0.4205
15	323.8	1.228	158.3	0.22787	0.6344	0.4205
16	360.2	5.629	2663	8.648		0.09058
25	265	2791	-166	-1.204		1.996
26	265	2791	-326	-1.808		0.9828
27	263.2	2649	-326	-1.807		0.9828

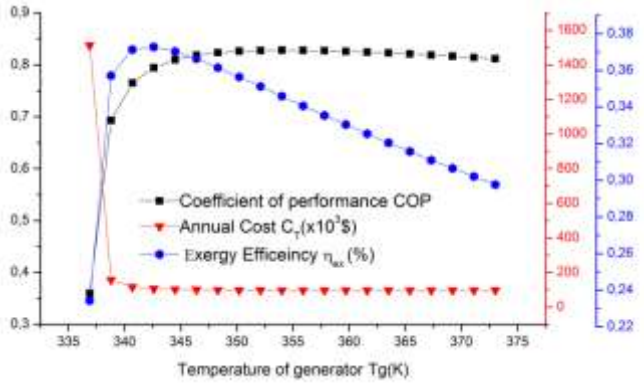

Figure5. The effect of generator temperature on the coefficient of performance, the exergy efficiency, and the annual cost of proposed cycle.

These trends can be explained as follows. In the first interval (Tg = 336–343 K), the difference between the strong and weak solutions is small. To maintain constant absorbed heat in the cascade heat exchanger, a large solution flow is required due to the constant water vapor mass flow in the condenser, expansion valve No. 1, and the cascade heat exchanger. Heating this solution for vapor production requires more energy at lower (Tg). In the second interval (Tg = 343–373 K), the difference between the strong and weak solutions stabilizes, resulting in a corresponding stabilization of generation heat, COP, and annual cost, as shown in Figure 6.

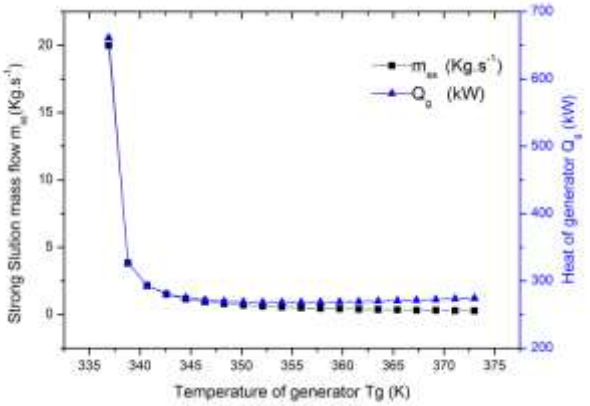

Figure6. The variation of heat of generator and the strong solution mass flow with generator temperature.

4.4. Exergy Analysis of ECACC

Figure 7 illustrates the exergy destruction of the main components of the ECACC. The absorber, generator, cascade heat exchanger, solution heat exchanger, and condenser account for the majority of exergy destruction, followed by the compressor and ejector. Among these components, the heat exchangers exhibit the highest exergy destruction. To enhance system performance and reduce exergy losses, the heat exchangers should be optimized in two ways: first, by improving overall heat transfer, which may include reducing the mass flow of the transported fluid; and second, by using construction materials with thermophysical properties better suited for heat exchange, such as high thermal conductivity and low heat capacity and density.

Figure 8 presents the exergy destruction percentages of the different ECACC components. The new components—the ejector and liquid–vapor heat exchanger—contribute only 8.47% of the total exergy destruction, compared with the conventional CACC reported by Du et al. [2], while improving the COP and exergy efficiency from 0.58 and 0.22 to 0.82 and 0.329, respectively. Therefore, the new configuration is strongly recommended for cascade compression–absorption cycles.

Figure 9 shows the investment costs of the different ECACC components. The results indicate that the heat exchangers are the most expensive components. Using materials with high overall heat transfer coefficients can reduce the required heat exchange area, lower costs, and decrease the total system investment.

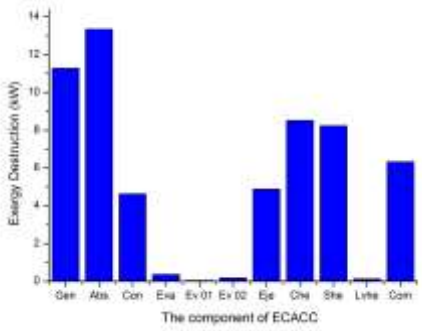

Figure 7. The exergy destruction of different components of ECACC.

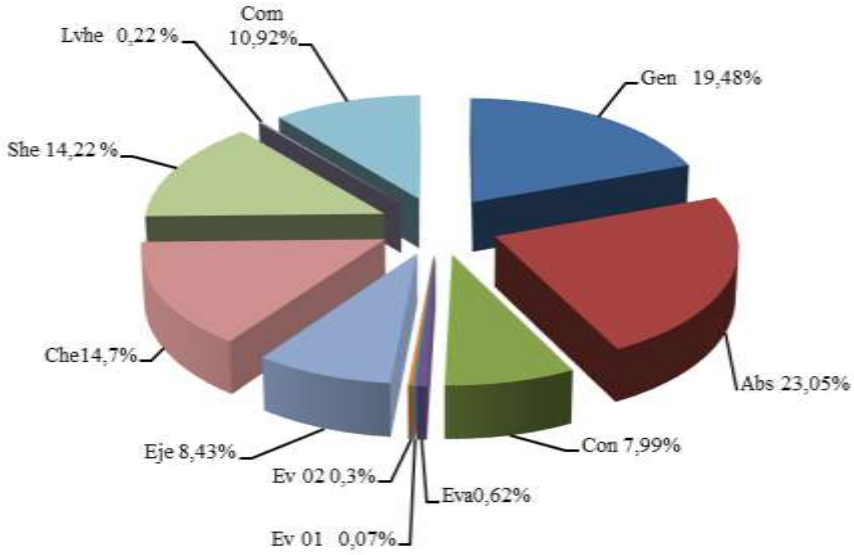

Figure8. The participation percentage of different components of ECACC in the exergy destruction of the cycle.

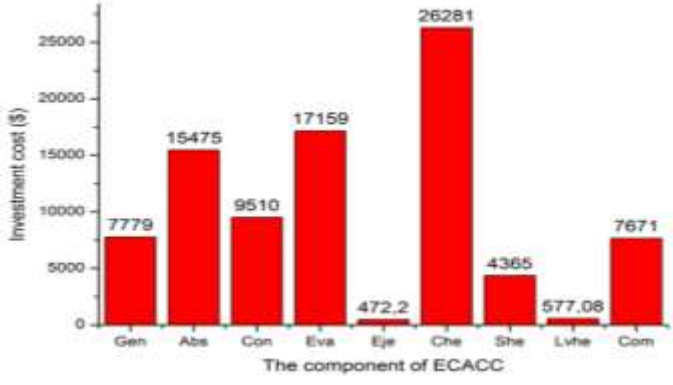

Figure9. The investment cost of different components of ECACC.

5. CONCLUSIONS

In this study, a novel ejector compression–absorption cascade cycle (ECACC) was proposed and comprehensively analyzed. The developed thermodynamic model was validated using both numerical simulations and experimental data from the literature, ensuring the reliability and accuracy of the results. Based on the detailed analysis and performance evaluation, the main conclusions of this work can be summarized as follows:

- The results demonstrate that the refrigerant R744 achieves the highest coefficient of performance (COP) and exergy efficiency among the eleven working fluids examined.

- The optimal performance of the proposed ECACC is achieved at a generator temperature of 72 °C, enabling effective utilization of low-grade renewable thermal energy sources, such as solar heat.
- For every operating condition, there exists an optimal generator temperature that maximizes both COP and exergy efficiency while minimizing annual operating costs. The dominant sources of irreversibility are identified in the heat exchangers, absorber, generator, cascade heat exchanger, solution heat exchanger, and condenser, followed by the compressor and ejector.
- The inclusion of the ejector and liquid–vapor heat exchanger in the conventional compression–absorption cascade configuration accounts for approximately 8.47% of the total exergy destruction. Nevertheless, these additional components significantly enhance overall system performance, increasing the COP from 0.58 to 0.82 and the exergy efficiency from 0.22 to 0.329.
- The heat exchanger surface areas are shown to play a crucial role in determining the investment cost of the proposed cycle, highlighting the importance of optimal thermal design in achieving both energetic and economic efficiency.

The results of this study highlight the technical feasibility and thermodynamic advantages of the proposed ECACC system. The developed model closely matches available experimental and numerical data, confirming its reliability. With improved COP and exergy efficiency compared to conventional systems, the ECACC configuration is recommended for applications utilizing low-grade thermal energy sources. The integration of the ejector enhances overall performance while weakly increasing exergy destruction, making the ECACC a promising solution for sustainable cooling and heating technologies.

Competing Interests

The author declares that they have no conflict of interest.

References

[1] Khelifa S., Korichi M., and Elsaid K., Thermodynamic and thermo-economic analysis of compression-absorption cascade refrigeration system using low-GWP HFO fluids powered by geothermal energy, International Journal of Refrigeration, 2018, 94.
[2] Du Y., Chi C., and Wang X., Energy, exergy, and economic analysis of compression-absorption cascade refrigeration cycle using different working fluids, Energy Storage and Saving, 2024, 3(2), pp. 87-95.
[3] Khan Y., Naqib-Ul-Islam S.M., Faruque M.W., and Ehsan M.M., Advanced Cascaded Recompression Absorption System Equipped with Ejector and Vapor-Injection Enhanced Vapor Compression Refrigeration System: ANN based Multi-Objective Optimization, Thermal Science and Engineering Progress, 2024, 49, pp. 102485.
[4] Zhang H., Pan X., Chen J., and Xie J., Energy, exergy, economic and environmental analyses of a cascade absorption-compression refrigeration system using two-stage compression with complete intercooling, Applied Thermal Engineering, 2023, 225, pp. 120185.
[5] Regulation (EU) No 517/2014 of the European Parliament and of the Council of 16 April 2014 on fluorinated greenhouse gases and repealing Regulation (EC) No 842/2006 Text with EEA relevance, E. Parliament, Editor, 2014.
[6] Final Rule - Protection of Stratospheric Ozone: Change of Listing Status for Certain Substitutes under the Significant New Alternatives Policy Program 2016, United State EnvironmentaL Protection Agency.
[7] Caliskan O., Bilir Sag N., and Ersoy H.K., Thermodynamic, environmental, and exergoeconomic analysis of multi-ejector expansion transcritical CO2 supermarket refrigeration cycles in different climate regions of Türkiye, International Journal of Refrigeration, 2024, 165, pp. 466-484.
[8] Song J., Li X.-s., Ren X.-d., and Gu C.-w., Performance improvement of a preheating supercritical CO2 (S-CO2) cycle based system for engine waste heat recovery, Energy Conversion and Management, 2018, 161, pp. 225-233.
[9] Zhi L.-H., Hu P., Chen L.-X., and Zhao G., Thermodynamic analysis of an innovative transcritical CO2 parallel Rankine cycle driven by engine waste heat and liquefied natural gas cold, Energy Conversion and Management, 2020, 209, pp. 112583.
[10] Cimsit C., Ozturk I.T., and Kincay O., Thermoeconomic optimization of LiBr/H2O-R134a compression-absorption cascade refrigeration cycle, Applied Thermal Engineering, 2015, 76, pp. 105-115.
[11] Seyfouri Z. and Ameri M., Analysis of integrated compression–absorption refrigeration systems powered by a microturbine, International Journal of Refrigeration, 2012, 35(6), pp. 1639-1646.
[12] Bahrami H.-R. and Fazli S., Comparative exergy and energy analyses of compression-absorption cascade refrigeration cycles with varied configurations and ejector implementations, Proceedings of the Institution of Mechanical Engineers, Part E: Journal of Process Mechanical Engineering, 2024.
[13] Dixit M., ENERGY AND EXERGY ANALYSIS OF ABSORPTION- COMPRESSION CASCADE REFRIGERATION SYSTEM, Journal of Thermal Engineering, 2016, 2.
[14] Özen D.N. and Yağcıoğlu K.Ç., Thermodynamic and Exergy Analysis of an Absorptıon Cooling System for Different Refrigerants, El-Cezeri, 2020, 7(1), pp. 93-103.
[15] Liu Z., Zeng Z., Deng C., and Xie N., Advanced Exergy Analysis of an Absorption Chiller/Kalina Cycle Integrated System for Low-Grade Waste Heat Recovery, Processes, 2022, 10, 2608, DOI: 10.3390/pr10122608.
[16] Kumar A. and Modi A., Energy and exergy analysis of a novel ejector-assisted compression–absorption–resorption refrigeration system, Energy, 2023, 263, pp. 125760.
[17] Yuksel Y.E., Thermodynamic and performance evaluation of an integrated geothermal energy based multigeneration plant, El-Cezeri, 2020, 7(2), pp. 381-401.
[18] Tunay M., Okwose C.F., Abid M., Adedeji M., Adebayo V.O., Ratlamwala T.A.H., and Rabbani M.A., Thermodynamic and Optimization Comparison of a Solar-Powered Compressor-Assisted Combined Absorption Refrigeration and Power Systems, El-Cezeri, 2024, 11(3), pp. 267-282.
[19] Faruque M.W., Khan Y., Nabil M.H., and Ehsan M.M., Parametric analysis and optimization of a novel cascade compression-absorption refrigeration system integrated with a flash tank and a reheater, Results in Engineering, 2023, 17, pp. 101008.

[20] Mukhtar H. and Ghani S., Hybrid Ejector-Absorption Refrigeration Systems: A Review, Energies, 2021, 14, pp. 6576.
[21] Huang B.J., Chang J.M., Wang C.P., and Petrenko V.A., A 1-D analysis of ejector performance, International Journal of Refrigeration, 1999, 22(5), pp. 354-364.
[22] Soytürk G., Çelik Toker S., and Kızılkan Ö., Thermodynamic Analysis of Ammonia Based Direct Steam Generation Trigeneration System, El-Cezeri, 2022, 9(2), pp. 721-739.
[23] Gomri R., Simulation study on the performance of solar/natural gas absorption cooling chillers, Energy Conversion and Management, 2013, 65, pp. 675-681.
[24] Mebarki B., Performance Investigation of Ejector Assisted Power Cooling Absorption Cycle, International Journal of Thermodynamics, 2023, 26(3), pp. 15-24.
[25] Milovancevic U., Jacimovic B., Genic S., El-Sagier F., Otović M., and Stevanovic S., Thermoeconomic analysis of spiral heat exchanger with constant wall temperature, Thermal Science, 2018, 2018, pp. 150-150.
[26] Baghernejad A. and Yaghoubi M., Thermoeconomic Methodology for Analysis and Optimization of a Hybrid Solar Thermal Power Plant, International Journal of Green Energy - INT J GREEN ENERGY, 2012, 10.
[27] Chinnappa J.C.V., Crees M.R., Srinivasa Murthy S., and Srinivasan K., Solar-assisted vapor compression/absorption cascaded air-conditioning systems, Solar Energy, 1993, 50(5), pp. 453-458.
[28] Cimsit C. and Ozturk I.T., Analysis of compression–absorption cascade refrigeration cycles, Applied Thermal Engineering, 2012, 40, pp. 311-317.
[29] Caliskan O. and Ersoy H.K., Energy analysis and performance comparison of transcritical CO2 supermarket refrigeration cycles, The Journal of Supercritical Fluids, 2022, 189, pp. 105698.
[30] Jain V., Sachdeva G., and Kachhwaha S.S., Energy, exergy, economic and environmental (4E) analyses based comparative performance study and optimization of vapor compression-absorption integrated refrigeration system, Energy, 2015, 91, pp. 816-832.
[31] Aminyavari M., Najafi B., Shirazi A., and Rinaldi F., Exergetic, economic and environmental (3E) analyses, and multi-objective optimization of a CO2/NH3 cascade refrigeration system, Applied Thermal Engineering, 2014, 65(1), pp. 42-50.
[32] Gebreslassie B.H., Guillén-Gosálbez G., Jiménez L., and Boer D., Design of environmentally conscious absorption cooling systems via multi-objective optimization and life cycle assessment, Applied Energy, 2009, 86(9), pp. 1712-1722.
[33] Wang J., Zhai Z., Jing Y., and Zhang C., Particle swarm optimization for redundant building cooling heating and power system, Applied Energy, 2010, 87(12), pp. 3668-3679.
[34] Cheng Y., Wang M., and Yu J., Thermodynamic analysis of a novel solar-driven booster-assisted ejector refrigeration cycle, Solar Energy, 2021, 218, pp. 85-94.
[35] Yang Z., Feng B., Ma H., Zhang L., Duan C., Liu B., Zhang Y., Chen S., and Yang Z., Analysis of lower GWP and flammable alternative refrigerants, International Journal of Refrigeration, 2021, 126, pp. 12-22.
[36] Miraj Arefin M., Mondal D., and Ashraful Islam M., Optimizing cascade refrigeration systems with low GWP refrigerants for Low-Temperature Applications: A thermodynamic analysis, Energy Conversion and Management: X, 2024, 24, pp. 100722.
[37] Sánchez D., Andreu-Nácher A., Calleja-Anta D., Llopis R., and Cabello R., Energy impact evaluation of different low-GWP alternatives to replace R134a in a beverage cooler. Experimental analysis and optimization for the pure refrigerants R152a, R1234yf, R290, R1270, R600a and R744, Energy Conversion and Management, 2022, 256, pp. 115388.